SF2A 2006
D. Barret, F. Casoli, T. Contini, G. Lagache, A. Lecavelier, and L. Pagani (eds)

RELATIVISTIC HYDRO WITH AMRVAC AND SIMULATION OF ULTRA-RELATIVISTIC DYNAMICS

Z. Meliani[1], R. Keppens[2] and F. Casse[3]

Abstract. Our aim is to numerically investigate Gamma Ray Burst (GRB) afterglows in the context of a fireball model. This requires the accurate computation of relativistic hydrodynamic flows, with a need for Adaptive Mesh Refinement (AMR) due to the extreme demands for resolving thin ultra-relativistic 'shells' propagating over vast distances. Here, we concentrate on the precise propagation evolution of such relativistic shells in spherical symmetric, as well as axisymmetric 2D models.

For this purpose, we extended the AMRVAC software (Keppens et al. (2003)) with a capability to simulate special relativistic hydro scenarios. We use a robust second order, shock-capturing discretization in a finite volume treatment in combination with AMR. On the numerical level, we can ensure physical consistency between the primitive $(\rho, \vec{v}, p)$ and conservative variables at limited linear reconstruction stages, as well as at all AMR restriction and prolongation stages. Stringent test cases of special relativistic hydro shock problems benefit optimally from our AMR strategy.

1 Introduction

GRBs are the most powerful explosions in the universe (for a recent review see e.g. Meszaros (2006)). An important advance in our understanding of GRBs started with the discovery and detailed investigation of their long-lasting "Afterglow" counterparts in X-Ray, optical, and radio wavelengths. In this paper we investigate relativistic dynamics in a fireball model, in both one and two dimensional settings. In this fireball model, a compact GRB source releases a large amount of energy in a very short timescale, ultimately producing a very thin shell around the source expanding with ultra-relativistic velocity with all its energy converted to kinetic energy. The resulting cold shell continues to expand and interacts with the circumburst medium in a relativistic shock-dominated scenario. As the shell sweeps up the surrounding matter it decelerates, and the associated radiation shifts in wavelength. Here, we concentrate on the precise propagation evolution of the relativistic shell in spherical symmetric, as well as axisymmetric 2D models. This will be coupled to consecutive quantifications of the spectral evolution of the produced afterglow radiation in future work.

2 Relativistic Hydrodynamic equations

The special relativistic hydrodynamic evolution of a perfect fluid is governed by the conservation of the number of particles, and energy-momentum conservation. These two conservation laws can be written as

$$\left(\rho\, u^{\mu}\right)_{\mu} = 0\,, \quad T^{\mu\nu}_{\mu} = 0\,. \tag{2.1}$$

where ρ, $\vec{u} = (\gamma, \gamma\,\vec{v})$, and $T^{\mu\nu} = \rho\, h\, u^{\mu}\, u^{\nu} + p\, g^{\mu\nu}$ define, respectively, the proper density, the four-velocity and the stress-energy tensor of the perfect fluid. Their definition involves the Lorentz factor γ, the fluid pressure p, and the relativistic specific enthalpy $h = 1 + e + p/\rho$ where e is the specific internal energy. For the (inverse) metric $g^{\mu\nu}$, we take the Minkowski metric. Units are taken where the light speed equals unity.

[1] FOM-Institute for Plasma Physics Rijnhuizen, Nieuwegein
[2] Centre for Plasma Astrophysics, K.U.Leuven; FOM-Institute for Plasma Physics Rijnhuizen, Nieuwegein; Astronomical Institute, Utrecht University
[3] AstroParticule & Cosmologie (APC)

These equations can be written in conservative form involving the Cartesian coordinate axes and the time axis of a fixed 'lab' Lorentzian reference frame as

$$\frac{\partial U}{\partial t} + \sum_{j=1}^{3} \frac{\partial F^j}{\partial x^j} = 0\,. \tag{2.2}$$

The conserved variables can be taken as $U = \left[D = \gamma\,\rho, \vec{S} = \gamma^2 \rho\, h\, \vec{v}, \tau = \gamma^2 \rho\, h - p - \gamma\rho\right]^T$, and the fluxes are then given by $F = \left[\rho\gamma\,\vec{v}, \gamma^2 \rho\, h\, \vec{v}\vec{v} + p\,\mathbf{I}, \gamma^2 \rho\, h\vec{v} - \gamma\rho\,\vec{v}\right]^T$, where $\mathbf{I}$ is the 3×3 identity matrix.

To close this system of equations, we use the equation of state (EOS) for an ideal gas, which is the polytropic equation with the polytropic index Γ,

$$p \;=\; (\Gamma - 1)\;\rho\, e\,. \tag{2.3}$$

At each time step in the numerical integration, the primitive variables $(\rho, \vec{v}, p)$ involved in flux expressions should be derived from the conservative variables U resulting in a system of nonlinear equations. One can manipulate this system to a single equation for the pressure p,

$$\tau + D - \gamma(p)\, D - \frac{p + \Gamma p(\gamma(p)^2 - 1)}{\Gamma - 1} = 0\,, \tag{2.4}$$

which, once solved for p yields $\vec{v} = \frac{\vec{S}}{\tau + p + D}$. The nonlinear equation (2.4) is solved using a Newton-Raphson algorithm.

3 A Riemann test problem: ultra-relativistic wall impact

In a 1D test case, a cold fluid hits a wall and a shock front propagates back into the fluid, compressing and heating it as the kinetic energy is converted into internal energy. In fact, behind the shock the fluid becomes at rest. This test has an analytical solution in planar symmetry as considered by Blandford & McKee (1976), and the jump conditions are

$$p_2 = \rho_1\,(\gamma_1 - 1)\,(\gamma_1\Gamma + 1)\;, \quad \rho_2 = \rho_1 \frac{\gamma_1\Gamma + 1}{\Gamma - 1}\,, \quad v_{sh} = (\Gamma - 1)\,\frac{\gamma_1 v_1}{\gamma_1 + 1}\,. \tag{3.1}$$

These give the post shock pressure p_2 and density ρ_2 values in terms of the incoming density and Lorentz factor, together with the shock propagation velocity v_{sh}.

In our test we take the same initial conditions than in the recent paper by Zhang & MacFadyen, (2006), where a cold fluid $p = 10^{-4}$ with a density $\rho = 1.0$ has an impact velocity of $v_1 = \left(1.0 - 10^{-10}\right)$ (which corresponds to a Lorentz factor $\gamma = 70710.675$). The temperature after the shock becomes relativistic, and therefore we take the polytropic index $\Gamma = 4/3$. Hence the shock velocity is $v_{\rm sh} = 0.33332862$. The AMR simulation is done with 20 cells on the base level and 4 levels on the spatial range $0.0 < x < 1.0$. The result at $t = 2.0$, with the reflective wall at $x = 1$, is shown in Fig. 1. In this test, because of the constant state behind the shock, the maximum impact Lorentz factor that can be achieved numerically is limited only by the precision of the Newton-Raphson subroutine. This test is important to demonstrate its accurate treatment, in view of the intended simulations aimed at afterglows in GRBs. Indeed, in the shell-frame, the circumburst medium hits the dense shell with a high Lorentz factor. In a process similar to what is found in the above test, the kinetic energy of the impacting medium is converted to thermal energy, thus heating the external medium. Viewed in the lab frame where the shell is moving, the swept up circumburst medium will have similarly high Lorentz factor and will form a hot shocked layer ahead of the contact interface.

4 Models for relativistic dynamics in GRB afterglow phases

4.1 Isotropic explosions

In this simulation we consider an ISM with uniform density $n_{\rm ISM} = 1{\rm cm}^{-3}$. In this low density medium, we place a relativistic uniform shell at $R_0 = 10^{16}$cm from the central engine with a density $n_{\rm shell}$. According to Woods & Loeb (1995), the interaction of the shell with the ISM becomes appreciable at this distance, and has

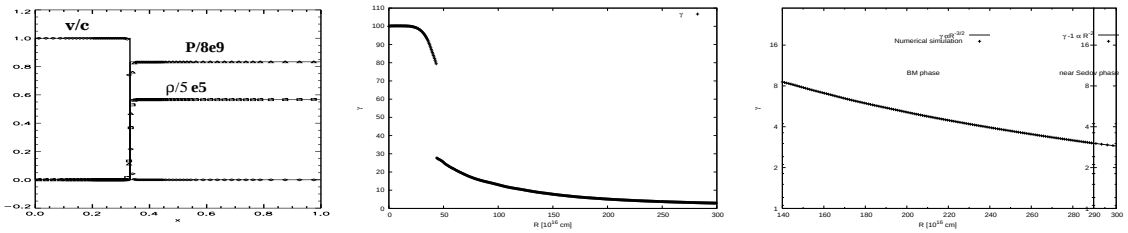

Fig. 1. Left: One-dimensional shock heating problem in planar geometry at $t = 2.0$. The computational grid consists of 20 zones with 4 levels of refinement. The exact solution is shown in solid lines. Middle & right panel: The variation of the Lorentz factor of the shell as a function of time. Middle: For the entire simulated time interval during which the shell propagates from $R_0 = 10^{16}$cm to $R = 300 \times R_0$. Right: during the times when the shell decelerates as in the self-similar Blandford-McKee phase.

an initial Lorentz factor of $\gamma = 100$ (note that $\gamma \geq 100$ in order to have a shell which is optically thin to gamma-rays Woods & Loeb (1995), Sari & Piran (1995)). We assume the energy $E = \gamma\, 4\,\pi\, R_0^2\, \delta\, n_{\rm shell}\, c^2 = 10^{52}$ergs, as we consider a burst produced in $t = 10$s.

The shell's lab-frame thickness at this position is set to $\delta \simeq R_0/\gamma^2 = 10^{12}$cm. The ISM and the shell are cold, and their initial pressure is set $p = 10^{-4} \times n_{ISM}\, m_p\, c^2$. This then yields a relativistic scenario where the energy of the thin shell is dominated by kinetic energy. In this simulation we use a constant polytropic index $\Gamma = 4/3$. The interaction shell-ISM is dominated by the appearance of a forward shock, across which the temperature of the swept up ISM becomes relativistic. In the shell itself, the weak internal thermal energy induces a weak spreading of the shell, i.e. the thickness of the shell slightly increases. For this simulation, we use an effective resolution of 1536000 zones valid at the highest allowed grid level 10. The shell is then resolved by about 153 cells. We need to use a very high resolution to avoid any numerical diffusion which may cause an artificial (i.e. not related to the thermal effect mentioned above) spreading of the shell. We made sure that we always use the highest grid level 10 for resolving the forward and associated reverse shock, as both are of prime importance to determine the precise deceleration time.

In this AMR simulation, we resolve all four regions which characterise the initial interaction between an outward moving relativistic shell and the cold ISM. These are (1) the region in front of the forward shock where ISM material is at rest, (2) the swept up shocked ISM region between the forward shock and the contact discontinuity between shell-ISM matter, with heated ISM matter that has passed through the forward shock, (3) the part of the shell material which has been traversed by the reverse shock, and (4) the part of the shell which is at yet non-shocked.

In this proceeding contribution, we focus on the deceleration of the shell as a direct consequence of the swept-up matter. The shell sweeps up a mass $M_{\rm shell}/\gamma$ at a distance $R_\gamma \sim 5.42 \times 10^{16}$cm. $M_{\rm shell} = \frac{E}{\gamma\, c^2}$ the initial mass of the shell. However, at this distance the reverse shock has only crossed about 5% of the initial shell. The near-total deceleration of the shell plus the shocked ISM matter takes place when the two shocks in the configuration convert an important fraction of the kinetic energy to thermal energy (this conversion in fact depends on whether the reverse shock is relativistic or classical). Note that the sweptup ISM receives both significant kinetic and thermal energy. In the first phase of the deceleration, the maximum Lorentz factor of the shell decreases gently from 100 at a distance $R \sim 2.5 \times 10^{17}$cm to 80 at a distance 4.3×10^{17}cm. At the former distance, the mass of swept up ISM is of the order of the initial mass of the shell.

A sudden deceleration of the shell happens at the latter distance 4.3×10^{17}cm from the central engine, where the Lorentz factor drops from $\gamma = 80$ to $\gamma = 30$. This drop of the maximum Lorentz factor that is seen in Fig. 1 marks the time where the reverse shock reaches the back end of the initially cold shell, meanwhile converting a fraction of its kinetic to thermal energy. Up to this time, the maximal Lorentz factor corresponds to the Lorentz factor of the non-shocked shell part. When the reverse shock completely has crossed the shell, the maximal Lorentz factor plotted then corresponds to the Lorentz factor of the shocked ISM-shell, which turns out to be 30. In the later stages, the extent of the shocked ISM layer situated between the front shock and the contact discontinuity becomes comparable to the thickness of a blast wave $R/4\gamma_{(2)}^2$ solution (Kobayashi & Sari, 2000). From this distance 14.0×10^{17}cm, the deceleration starts to follow the analytical solution of Blandford & McKee. The transition to the essentially non-relativistic Sedov-Taylor phase for blast wave evolution starts at a distance $R > 30 \times 10^{18}$cm, which is shifted from the analytical estimate given by $l \sim (E/n_{\rm ISM}\, m)^{1/3} \sim 10^{18}$cm. This difference can be understood from the fact that only the front part of the entire structure follows the analytic

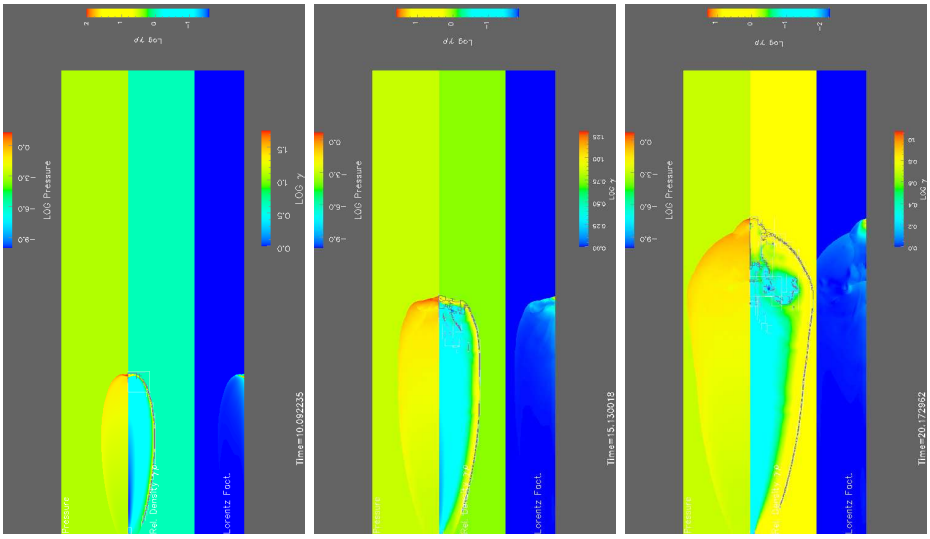

Fig. 2. The density, pressure and Lorentz factor contours at different times for the 2D shell simulation. Left: when the shell reach $R = 10^{17}$ cm. Middle: $R = 1.5 \times 10^7$ cm. Right: at $R = 2.0 \times 10^7$ cm .

self-similarity assumption.

4.2 Axisymmetric 2D shell geometries

As the explosions in reality will likely occur anisotropically, we need to consider ultra-relativistic shell dynamics in at least 2D settings. Assuming alignment along the polar regions of the source, the shell can be still assumed as axisymmetric, but has a prescribed initial opening angle. The resulting afterglow radiation will likely also be influenced by the precise multidimensional aspects of propagation of the jet in the ISM. We present 2D simulations of a relativistic cold shell, propagating in the uniform ISM with a density $n = 1\text{cm}^{-3}$. The simulated shell this time has an energy $E = 10^{49}$ergs and a Lorentz factor $\gamma = 100$. We start the simulation with a uniform shell of thickness $\delta = 10^{14}$cm at a distance $R_0 = 10^{16}$cm from the central engine. The half open angle of the shell is $\Delta\theta = 1°$, thus initialy, we have $\gamma > 1/\Delta\theta$. Also, we assume the initial velocity of this shell to be purely radial.

Fig. 2 shows the evolution of the Lorentz factor and density. As in the 1D case, in a first phase the shell propagates with a near-constant Lorentz factor and undergoes a weak thermal spread in the radial direction. The spreading in the bottom part of the shell is also affected by the appearance of a very low pressure and density region below the shell, as a near vacuum is left when the shell propagates upwards. In the top layers of the shell, it is due to the increase of the thermal energy in the zone between the contact discontinuity and the reverse shock. The non-shocked shell also spreads laterally with the initial velocity of order $v \sim 0.017\,c$. However, as soon as the reverse shock has crossed the entire shell, shell and shocked ISM start spreading sideways with lateral velocity of $v \sim 0.74c$. Due to this fast lateral expansion, the shell decelerates faster, since more matter gets accumulated.

We acknowledge financial support from the Netherlands Organization for Scientific Research, NWO grant 614.000.421, and for the use of computing facilities by NCF. ZM acknowledge financial support from APC, Paris 7.

References

Blandford, R. D. & McKee, D. G. 1976, Physics of Fluids, 19, 1130

Keppens, R. et al. 2003, Comp. Phys. Commun., 153, 317

Meszaros, P. 2006, Rep. Prog. Phys., 69, 2259

Sari, R. & Piran, T. 1995, ApJL, 455, L143

Kobayashi S. & Sari R. 2000, ApJ, 542, 819

Woods E. & Loeb A. 1995, ApJ, 453, 583

Zhang W. & MacFadyen, A.I. 2006, ApJSS, 164, 255